Replication of microchannel structures in WC–Co feedstock using elastomeric replica moulds by hot embossing process

Mohamed Lakdhar Sahli, Jean-Claude Gélin, Thierry Barrière

Replication of microchannel structures in WC–Co feedstock using elastomeric replica moulds by hot embossing process

M. Sahli *, J.-C. Gelin, T. Barrière

Femto-ST Institute, Applied Mechanics Dept., CNRS UMR 6174, ENSMM, 25030 Besançon cedex, France

Hot embossing is a net shaping process that is able to produce the micro components of polymers with intrinsic and complex shapes at lower cost compared with machining and injection moulding. However, the emboss of hard metals, such as WC Co, is more challenging due to their high thermal conductivity and ease of agglomera tion. Thus, a WC Co alloy mixed with a wax based binder feedstock was selected. The formed feedstock exhib ited pseudo plastic flow and was successfully embossed (green part). Here, we developed a novel process that is used to replicate polymer microfluidic chips while simultaneously reducing the channel surface roughness of the mould insert, yielding optical grade (less than 100 nm surface roughness) channels and reservoirs.
This paper concerns the replication of metallic microfluidic mould inserts in WC Co and the parameters associ ated with feedstock formation via a hot embossing process. A suitable formulation for micro powder hot embossing has been established and characterised by thermogravimetric analyses and measurements of mixing torques to verify and quantify the homogeneity of the proposed feedstocks. The relative density of the samples increased with processing temperature, and almost fully dense materials were obtained. In this work, the effects of the sintering temperature on the physical properties were systematically analysed. The evolution of the metal surface morphology during the hot embossing process was also investigated. The results indicate that the feed stock can be used to manufacture micro fluidic die mould cavities with a low roughness, proper dimensions and good shape retention. The shrinkage of the sintered part was approximately 19 24% compared with that of the brown part.

* Corresponding author.
E-mail address: Mohamed.sahli@ens2m.fr (M. Sahli).

1. Introduction

Recently, micro structured parts have been manufactured using several methods, including mechanical machining, lithographic processes, epitaxy and ion beam technologies. Most of these methods are relatively expensive, have time constraints and geometry limitations with poor dimensional accuracy, and are sometimes hindered by excessive waste material. For example, micro milling is a relatively simple technique that is widely used to manufacture hard moulds and can produce channel features down to 50 μm; however, the surface roughness is generally quite poor and insufficient for most microfluidic applications [1 5].

Today, other micro manufacturing technologies [6 8], such as micro injection moulding [9 12], casting [13,14] and micro hot embossing [15,16], have been developed for different applications such as biochemical MEMS. The hot embossing process (HE) is one of the most important and promising technologies that has been recently developed. This process is commonly used for the manufacturing of micro electro mechanical systems (MEMS), micro lenses and micro optical elements, especially in polymeric materials [17 19]. The technique often uses hard tools with a high surface roughness (often on the micron scale) and micro channels that generate a decrease in the overall efficiency of fluidic flow and often compromise the optical quality [20 22]. These micro fluidic devices are extensively used for various types of bio chemical analyses such as waste water monitoring, identification of environmental toxins, targeted drug delivery, analysis of DNA sequences and point of care diagnostics [23 26]. Therefore, powder hot embossing is a promising net shaping process that is able to meet the all of these requirements [27 30]. This technique opens the path to many industrial applications due to the high homogeneity of the embossing on large surfaces [31]. The technology and knowledge behind powder hot embossing involve a combination of powder metallurgy and the micro hot embossing process.

In general, powder hot embossing consists of four stages: mixing of the powder and binder to prepare the feedstock, hot embossing using elastomeric stamps to replicate the hard mould inserts, debinding to remove the binder constituents and sintering to promote the diffusion of the powder to achieve the required properties [32,33]. However, the life of the mould inserts could also be a very important aspect to consider. During the repetitive cycle of micro replications (injection, hot embossing…), the mould inserts must be able to resist the high clamping force of the machine and fatigue, abrasion, etc. Thus, we must select tungsten carbide cobalt (WC Co) for elaboration of our micro fluidic mould inserts. Tungsten carbide cobalt is an alloy with a hard ceramic phase, tungsten carbide (WC), and is expensive and extremely difficult to machine due to its high hardness and ductile metallic phase, cobalt (Co) [34,35]. Thus, most WC Co is produced through powder metallurgy processes, such as powder compaction. The important properties of WC Co are its hardness, strength, high breaking and beating ductility and high electrical and thermal conductivity [36,37]. By varying the metallic cobalt content and the tungsten carbide grain size, important properties of the alloy can be specifically adapted. Thus, the two objectives of this study are to investigate the micro replication by hot embossing and the effect of the sintering temperature on the mechanical and physical properties of the sintered mould insert.

In this paper, innovative solutions are proposed and developed for manufacturing metallic tools to easily reproduce micro structured surfaces, with a lateral resolution less than 100 nm for feedstocks with very low viscosity. The recent interest in powder hot embossing stems from the need to prepare a low cost mould cavity characterised by a lower surface roughness, a higher shape accuracy, great hardness and

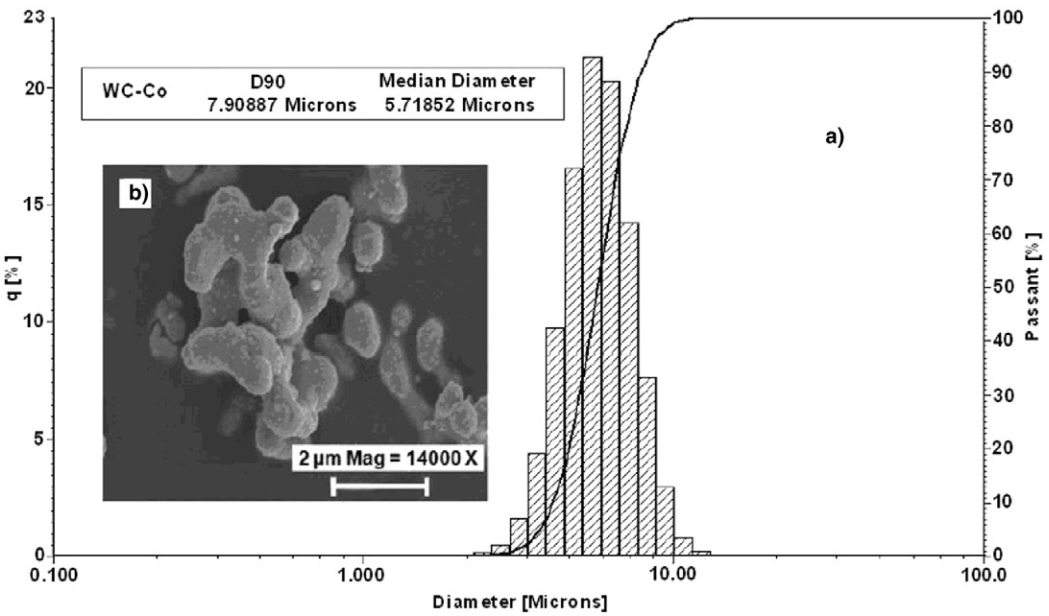

Fig. 1. (a) The particle size distribution for the WC–8 wt.% Co powders and (b) SEM image of WC–8 wt.% Co composite powder.

Table 1
Characteristics of the WC–Co powders.

Powder	Particle shape	d_{10}	d_{50}	d_{90}	Density	Tap density
WC–Co	Irregular	2.9 μm	5.71 μm	7.9 μm	9.74 g/cm^3	2.17 g/cm^3

Table 2
Material characteristics of the different binder components.

Binders	Density [g/cm^3]	Melting temperature [°C]
Stearic acid (SA)	0.89	70
Paraffin wax (PW)	0.91	60
Polypropylene (PP)	0.90	160

better dimensional stability. WC Co powders were mixed with a polypropylene based binder. The mixture was then forced to fill an elastomeric mould under low pressure and allowed to cool before being release from the mould cavity. This process produced dense and strong green parts. The binder was removed during the debinding to form brown parts, and then, the final WC Co replicas were obtained after sintering.

Many investigations have been conducted recently to investigate the polymer hot embossing process for microstructures. Lin et al. [38] investigated the pressure distributions on the polymer surface during the hot embossing process. The results indicated that the quality of a product manufactured by hot embossing is affected by its shrinkage during cooling. Therefore, the shrinkage of a polymer depends on the embossing pressure. Saha et al. [39] investigated the replication performance and limitation in the hot embossing process using a stainless steel micro mould. This work also investigated the coating properties at the sidewalls of the micro mould channels and the limitations of the Ti Al PTFE coatings for application in hot embossing. It was observed that the Ti Al PTFE coatings were a mixture of carbides, PTFE like material and amorphous carbon. The surface roughness of the coated micro moulds decreased with increasing PTFE concentration. These researchers also observed that the coated stainless steel micro moulds exhibited better replication performance compared with bare stainless steel micro moulds in terms of the quality of the polymeric micro fluidic devices fabricated. Shuhuai et al. [40] studied the principal factors affecting the final replication fidelity of the hot embossing process of glassy polymers for pattern replication. The relationship between the process condition and final quality was thoroughly and systematically investigated. These researchers demonstrated that the most significant factor is the embossing temperature, and the experiment with these parameters produced good results. Li et al. [41] performed a series of experiments to investigate the processing of micro components by hot embossing. The results of their research identified that the replication accuracy strongly depends on the processing conditions and on the processing temperature and pressure in particular. Jena et al. [42] demonstrated that micro fluidic devices with high fidelity micro channels could be produced using a single step hot embossing process based on knowledge of the effect of the embossing temperature, embossing pressure, embossing time and polymer chain orientation in the film/substrate on micro replication. Sahli et al. [43] investigated and compared the

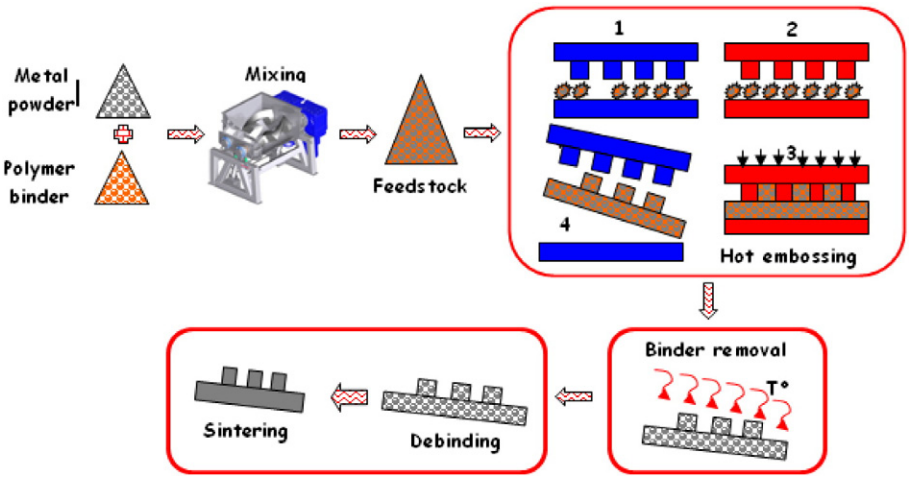

Fig. 2. A schematic illustration of the multi-stage sequential manufacturing process used for micro-structured die mould inserts, combining the hot embossing process and powder metallurgy process.

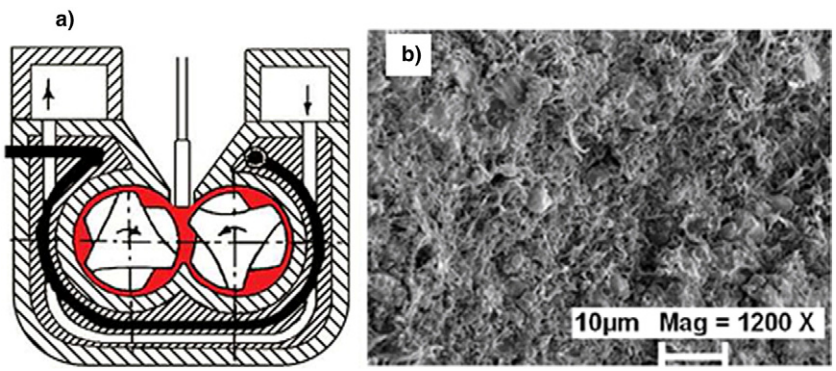

Fig. 3. (a) Scheme corresponding to a twin-screw Brabender® mixer and (b) SEM micrographs of the feedstock after mixing, including WC–Co (the solid loading equal to 44%).

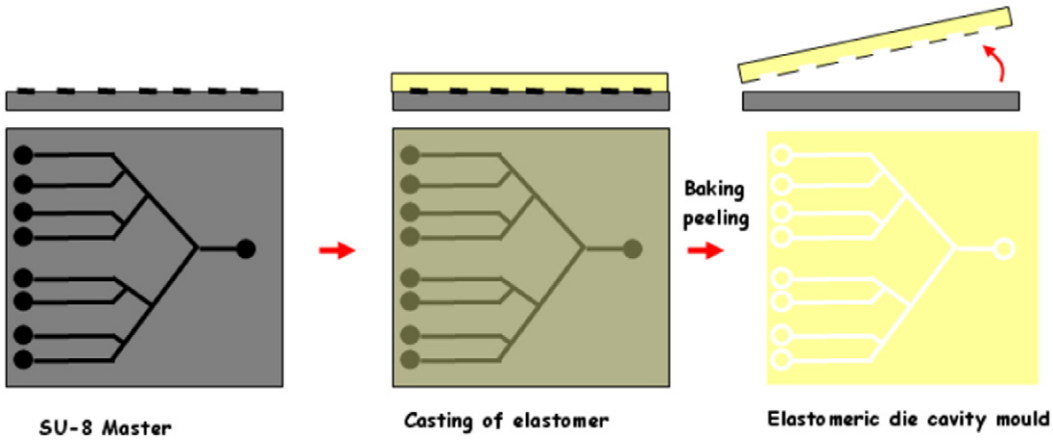

Fig. 4. Use of a SU-8 master for elastomeric casting.

replication quality of polymeric replicas obtained by filling microcavities. The results provided information on the reliability concerning the possi bility of replicating topographical surface geometries using both hot embossing and micro injection moulding processes.

Most studies in this field have been focused on thermoplastics [44 46] because of their extensive usage in various applications; however, there are few reports that describe the details and challenges of powder hot embossing. Recently, Fu et al. [47] investigated the manufacturing of 316L stainless steel cylindrical microstructure arrays using a silicon mould insert obtained by the hot embossing process. Their results demonstrated the effects of various embossing parameters on the filling of microcavities in the silicon mould insert and then de moulding of the micro structured parts. This study only focused on the replication of a microstructured array with an aspect ratio limited to 2. The study was limited to the use of 316L stainless steel with un known solid loading and binder percentages in its feedstock. Srivatsan et al. [48] performed an investigation of the effect of powder particle sizes on the resulting microstructures, including the presence and dis tribution of the porosity, cracks, density and micro hardness of tungsten carbide pieces. Three different particle sizes were selected and used to prepare the tungsten carbide samples. The results revealed that pulsing of the powders before consolidation led to higher density and micro hardness values compared with those obtained by consolidating the powders without pulse conditions.

The powder hot embossing process is adapted from the hot embossing process with certain technological adaptations; thus, this process is in a developmental stage. This paper attempts to in vestigate the feasibility of using WC Co powder for the manufacture of micro fluidic mould inserts using the powder hot embossing process. Thus, the flow properties of the feedstock are evaluated, and the main challenges encountered during hot embossing, debinding and sintering are described.

In this work, the relation between the embossing process and the feedstock properties was investigated in detail. The effects of the embossing temperature and pressure on the filling rates were systemat ically analysed the roughness surface morphology during the sintering stage was also studied. Therefore, the present work also analyses the shrinkages, densities and Vickers hardness values of the micro fluidic specimens.

2. Materials and methods

2.1. Materials

Fine powders of cobalt tungsten carbide with 19.9% WC (WC Co) were used to develop the mixtures dedicated to the hot embossing pro cess. The powders were characterised to have an average particle size of approximately 6 μm. Fig. 1a presents a photograph of the cobalt tungsten carbide powder particle distribution. The powders were provided by Eurotungstene Company® (Eramet) with densities equal to 9.74 $g \cdot cm^{-3}$. Fig. 1b presents SEM images of the WC 8 wt.% Co pow der. Before mixing, the powders were dried in a vacuum oven at a tem perature of 120 °C for 5 h to remove any moisture. WC Co feedstocks based on 40 to 75% solid loadings (by volume) were elaborated using a twin screw mixer. The binder system used in this study consists of stearic acid (SA), paraffin wax (PW) and polypropylene (PP). The composition of the binder corresponds to the ratio of PP:PW:SA given as relative fractions 40:55:5. The characteristics of the binder systems and raw powders are listed in Tables 1 and 2.

2.2. Experimental procedures

The proposed approach combines the hot embossing process and re lated powder metallurgy processes. This approach was developed for the rapid manufacturing of high quality metallic replicas on elastomeric moulds, as illustrated in Fig. 2. In this process, the metallic powders are mixed with a polymeric binder system, which mainly includes thermo plastic polymers. The resulting mixture is called a feedstock and is then embossed in the mould to achieve the required shapes. Then, the binder is removed during thermal debinding, and the powder is sintered, yield ing the full density necessary to provide the required mechanical prop erties and geometric size within the same time that a certain amount of shrinkage occurs.

2.2.1. Mixing tests

Experiments related to the mixing of binders and feedstocks were performed using a twin screw Brabender® Plastograph EC mixer with a pair of rotor blades connected with appropriate software to measure the mixing torque (see Fig. 3a). This equipment has a chamber volume

Table 3
Material characteristics of the different silicones.

Silicones	Mixing ratio A:B	Viscosity at 23 °C [Pa·s]	Density at 23 °C [g/cm^3]	Hardness Shore A
M4370 A/B	9:1	8.0	1.43	55
M4118 A/B	1:1	2.5	1.10	20
M4125 A/B	1:1	6.0	1.05	25
M4643 A/B	9:1	25.0	1.35	48
M4470 A/B	3	10.0	1.44	60
Sylgard 160	1:1	8.7	1.57	56
Sylgard 164	1:1	8.9	1.57	61
Sylgard 170	1:1	2.8	1.38	45
Sylgard 182	10:1	4.5	1.03	51
Sylgard 184	10:1	4.5	1.03	48

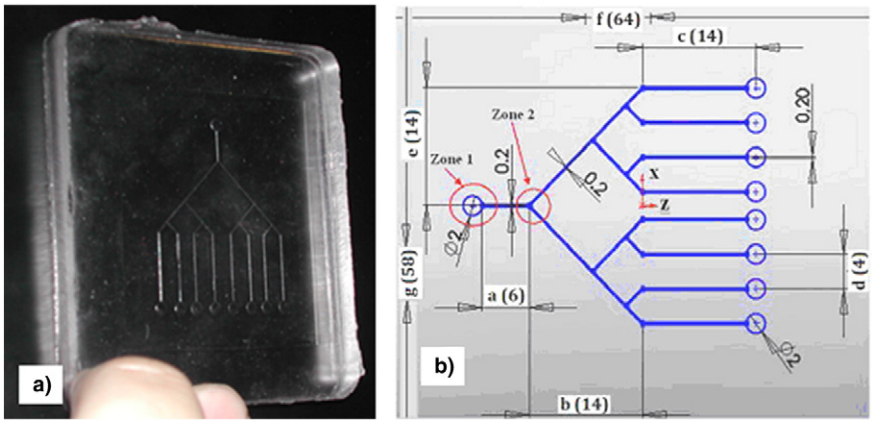

Fig. 5. a) Pattern geometry of the elastomeric die cavity mould and b) description of the mould dimensions and micro-fluidic geometries.

of 55 cm^3, and 73% of this volume was used for the tests. The mixing temperature was selected based on the melting point of polypropylene (T_f = 160 °C) and was set below the degradation temperature of paraf fin wax (T_d = 250 °C) and stearic acid (T = 180 °C). This temperature allowed complete melting and prevented binder degradation.

The same processing conditions were used for each mixture, which consist of the mixing temperature, mixing time and mixing rotation speed of 180 °C, 30 min and 30 rpm, respectively. The powders were loaded when the temperature was stabilised at the required mixing temperature to facilitate homogeneous mixing of the powder and bind er components. During a mixing test, the mixture homogeneity can be evaluated through the analysis of the mixing torque curves. Uniform mixing is achieved when the torque reaches a stable and steady state value. Fig. 3b presents scanning electron microscope (SEM) images of the cobalt tungsten carbide feedstock powders after the mixing stage. Finally, the feedstocks were granulated into small pellets for rheology characterisation and were then used in the hot embossing to make ac curate micro fluidic replicas.

2.2.2. Elastomeric mould replication

A master is made of the microstructures patterned on the surface of a substrate covered with SU 8 photoresist. The master is typically pro duced using photolithography and is intended to serve as a mould for pouring silicone and create micro fluidic patterns on the elastomer. When the layer of silicone is peeled away, the layer contains the inverse of the original pattern embossed on the surface of the master, as illus trated in Fig. 4.

Transferring the micro fabricated features to an elastomeric mould conserves the resolution down to 1 μm [49] and allows for the produc tion of multiple and inexpensive copies of the mould and hundreds of uses without significant ageing.

In this study, several soft materials were selected in the casting of elastomeric replicas, such as room temperature vulcanising (RTV) silicones on master moulds fabricated from photoresists on silicon sub strates. Two criteria were imposed in our material selection, either too low of a viscosity for easy filling of mould cavities and a high Shore hard ness (Shore A) for minimal shrinkage and with less deformation of the flexible mould during replication by the hot embossing process. Based on these criteria, the Sylgard 182 was selected for the realisation of rep licas using cobalt tungsten carbide feedstocks by hot embossing (see Table 3).

The Sylgard 182 provided by Dow Corning® was used as the materi al for casting the elastomeric moulds. The silicone base and a catalyst were thoroughly mixed at a ratio of 10:1. Next, the silicone mixture was poured over the SU8/Si and cured at 70 °C for 4 h; after curing, the silicone was easily peeled from the SU 8/Si master. The elastomeric mould was then obtained with one face that contained all of the details of the original master (Fig. 5a and b). The manufacturing process details for the processing of the SU 8/Si and PDMS moulds are also described in [1,50 52].

The dimensions, surface roughness and surface topographies of the elastomeric mould inserts and the micro fluidic samples were deter mined using a mechanical profilometer (Tencor Alpha Step IQ) with a 5 μm diamond tip radius operated at a scanning speed of 5 μm/s over a length of 1 mm both inside and outside of the reservoir pattern (2 mm in diameter). The geometric details of interest in the die mould developed by casting were determined using a mechanical profilometer corresponding to the shapes illustrated in Figs. 6 and 7.

2.2.3. Hot embossing process

The elastomeric die cavity moulds were used for the hot embossing process to manufacture micro components using feedstocks based on polypropylene, paraffin wax and stearic acid (see Fig. 8). The embossed tests were gradually established and performed in two different cases. In the first case, the tools were heated at a temperature equal to 190 °C with 5 °C/s as the heating rate; additionally, the dwell time was 10 min, and the forming load was varied from 200 to 400 N. In the second case, the tools were heated from room temperature to a tem perature in the interval from 170 to 230 °C; the heating rate was 5 °C/s, while the forming force was slowly increased to a load of 400 N. The temperatures were near the highest melting temperature T_f ($T_{f\ PP}$ =

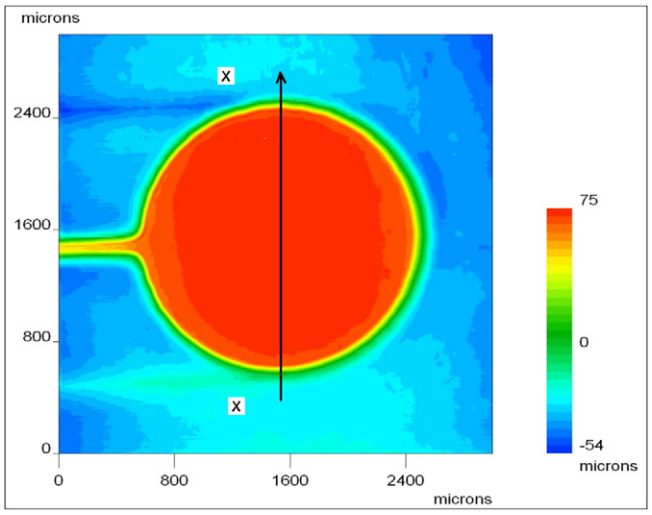

Fig. 6. 3D topographic imprints of the elastomeric die cavity mould realised by casting (unit: μm).

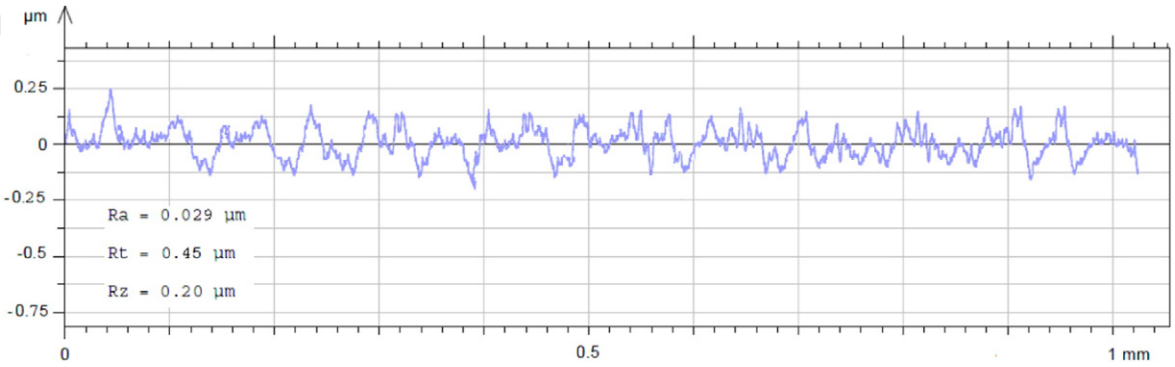

Fig. 7. Surface roughness profile graph of the elastomeric die cavity mould recorded by a mechanical profilometer.

160 °C) and the lowest degradation temperature T_d ($T_{d\text{-}SA}$ = 250 °C) of the binder system.

2.2.4. Thermal debinding and sintering steps

The debinding cycle was based on the TGA curve identified for the binder system. Slow heating at 1 °C/min under a H2/He atmosphere was first applied up to 350 °C for debinding, followed by heating up to 500 °C at 5 °C/min. The samples were maintained at these temperatures during for 30 min. Then, heating up to 1410 °C in vacuum at 3 °C/min or 1 °C/min was applied, where the samples were held for 60 min and then cooled down. Sintering is a useful method for manufacturing parts from powders by heating the material until its particles adhere to each other. However, the sintering temperature cannot exceed the melting point of the sintered based materials [53,54]. Fig. 9 summarises the processes as sociated with the debinding and sintering stages.

2.3. Thermal degradation properties

To determine the appropriate range of process parameters such as the mould temperature, forming temperature and debinding tempera tures, thermal characterisations of the binders were conducted. These characterisations included differential scanning calorimetry (DSC),

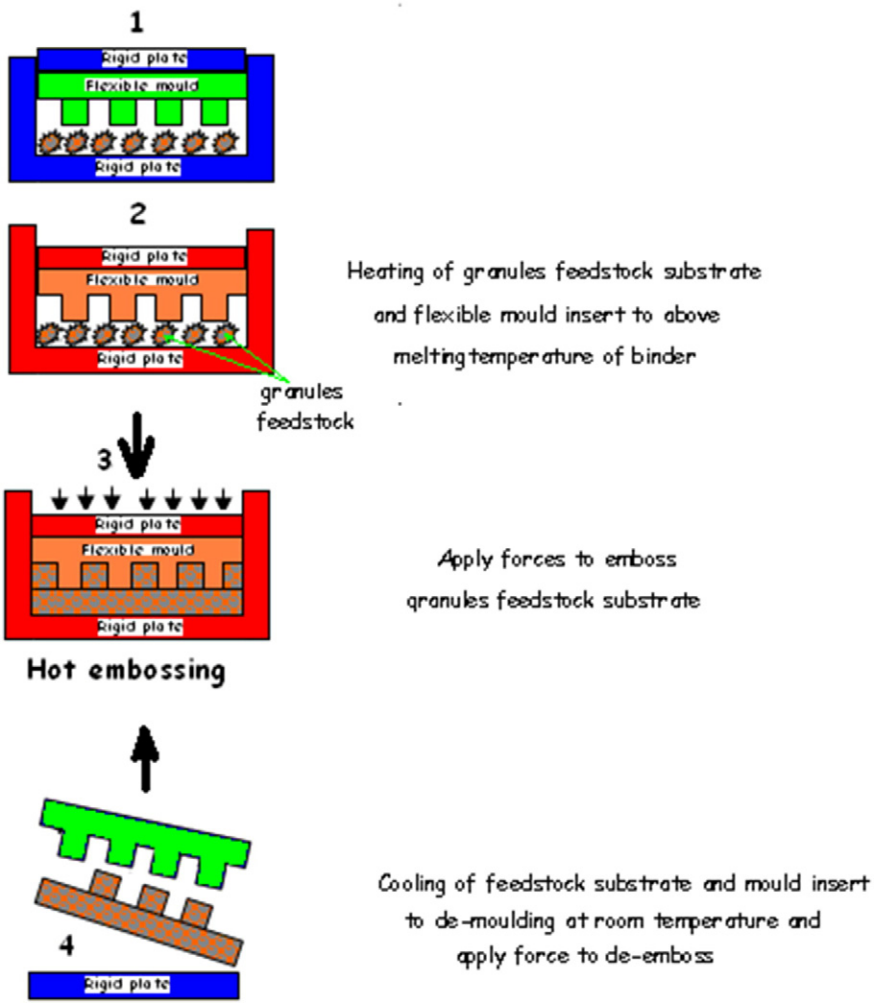

Fig. 8. Illustration of the hot embossing process to create micro-devices.

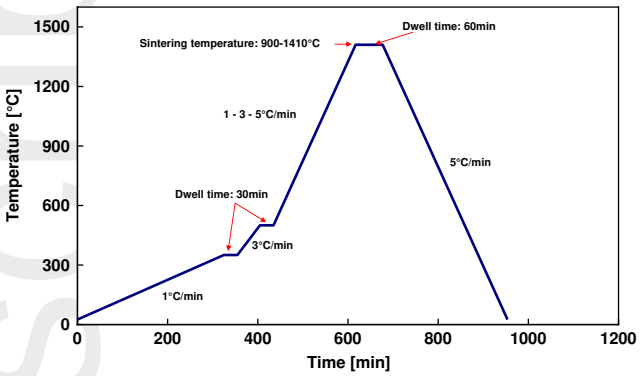

Fig. 9. The thermal debinding and sintering profiles.

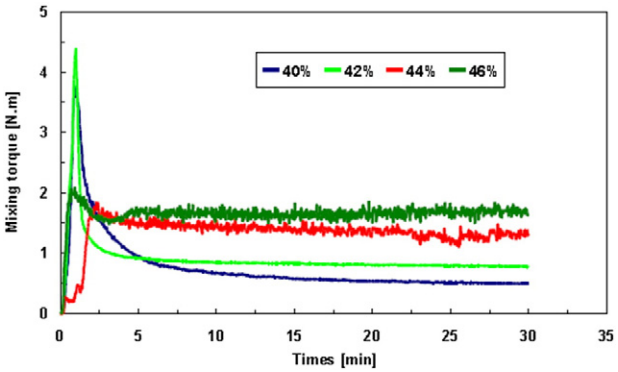

Fig. 12. Mixing torque vs. time considering four different powder loadings corresponding to cobalt tungsten carbide feedstocks, obtained from the mixing process (180 °C, 30 min and 30 rpm).

thermogravimetric (TGA) analysis and plan/plan rheometer testing. The DSC test was conducted on a Setaram Instrumentation Model DSC92 from 25 to 500 °C. A heating and cooling rate of 10 °C/min was used.

The degradation temperature ranges, as related to the binder com ponents in the powder/binder feedstocks, were obtained by thermogra vimetric analyses (TGA), which were performed using a Setaram Setsys

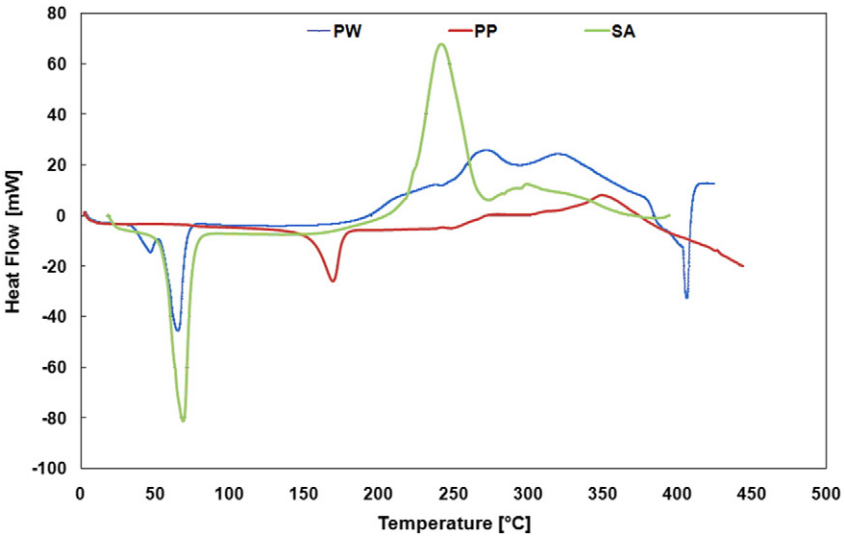

Fig. 10. Differential scanning calorimetry analysis of binders.

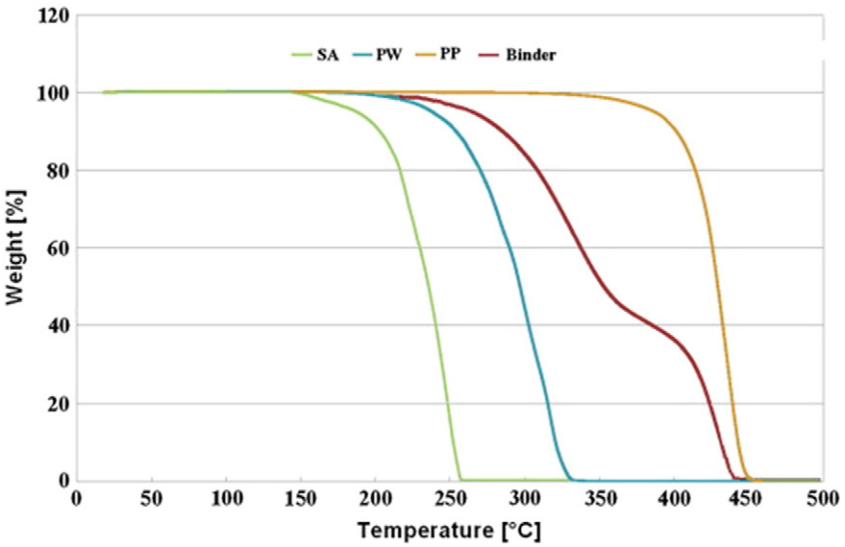

Fig. 11. TGA curves of all binders and the combined binder systems (PW 55%, PP 40%, SA 5%).

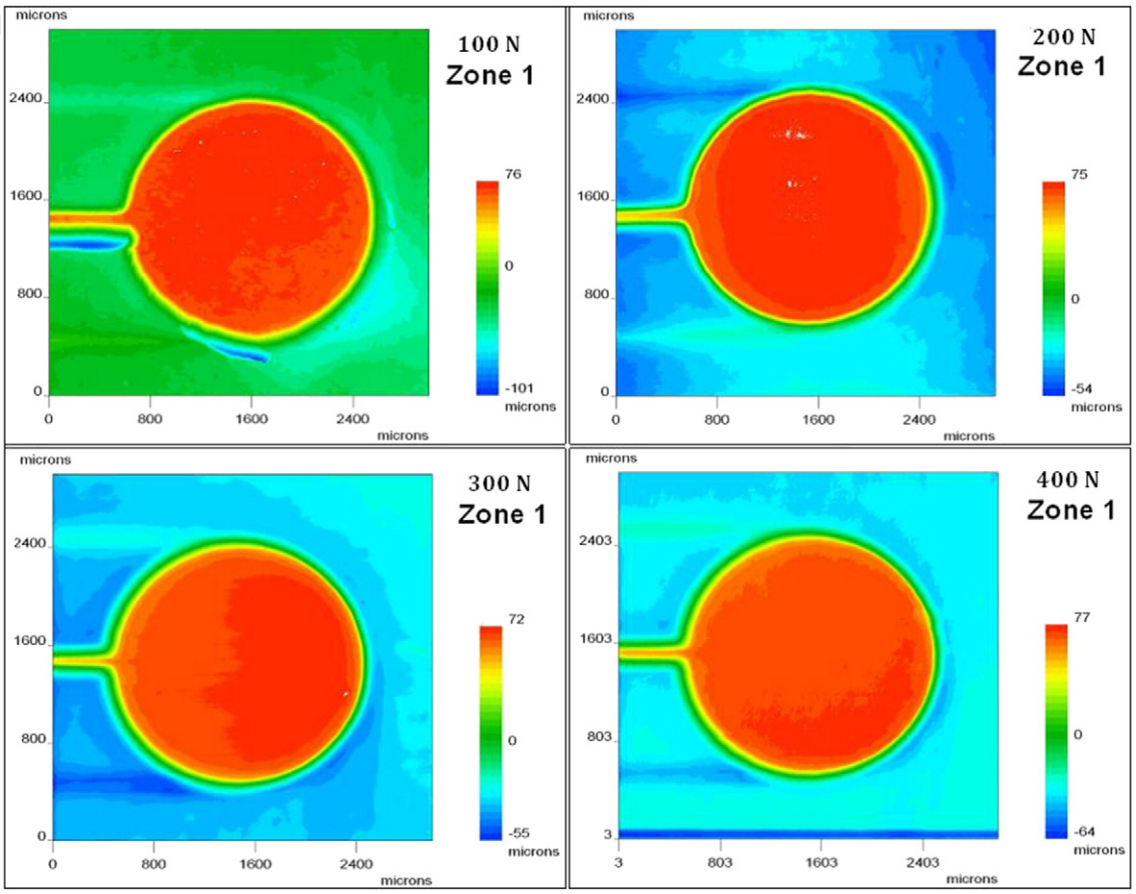

Fig. 13. 2D topographic imprints of the WC–Co feedstock replicas with a solid loading content of 40 vol.%, obtained at different forming loads (hot embossing temperature: 190 °C).

analyser® in the presence of a nitrogen atmosphere up to 500 °C at a heating rate of 5 °C/min.

3. Results and discussions

3.1. Fusion characteristics and thermal stability

Fig. 10 presents the differential scanning calorimetry results of the binders, for which three endothermic peaks, 60 °C, 70 °C and 160 °C, are observed during heating due to the melting of major binder components. From the differential scanning calorimetry result, the forming temperature for the hot embossing process should be higher than 160 °C to enable complete filling of the micro cavities.

Fig. 11 presents the TGA curves of the multi component binder and the individual binder components. In the TG curves collected above 250, 330 and 440 °C, the stearic acid, paraffin wax and polypropylene each finished approaches 0% (complete loss) at higher temperatures, which is the ideal case for binder removal in the debinding of metallic parts.

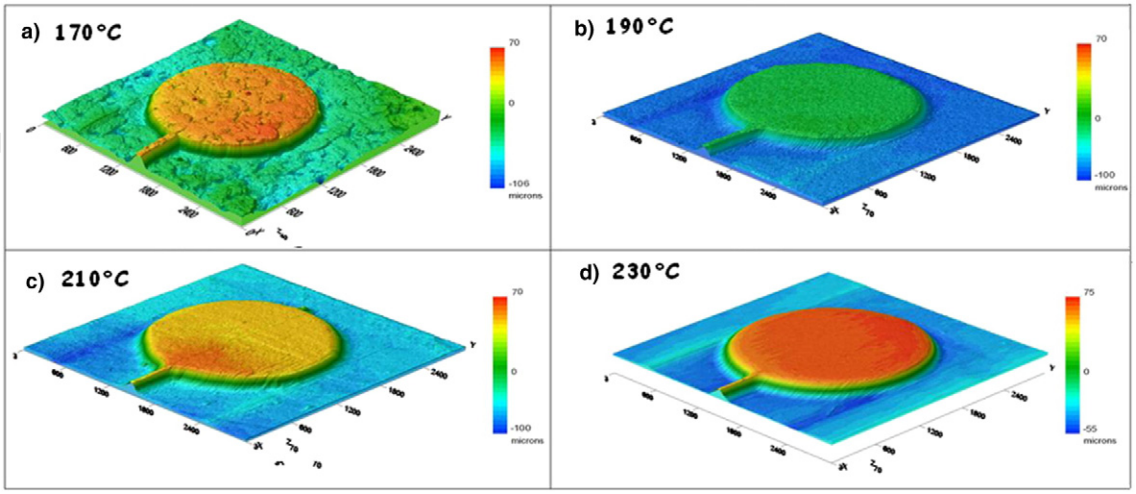

Fig. 14. 3D topographic imprints of WC–Co replicas with a solid content equal to 40 vol.%, obtained at various forming temperatures (units: μm).

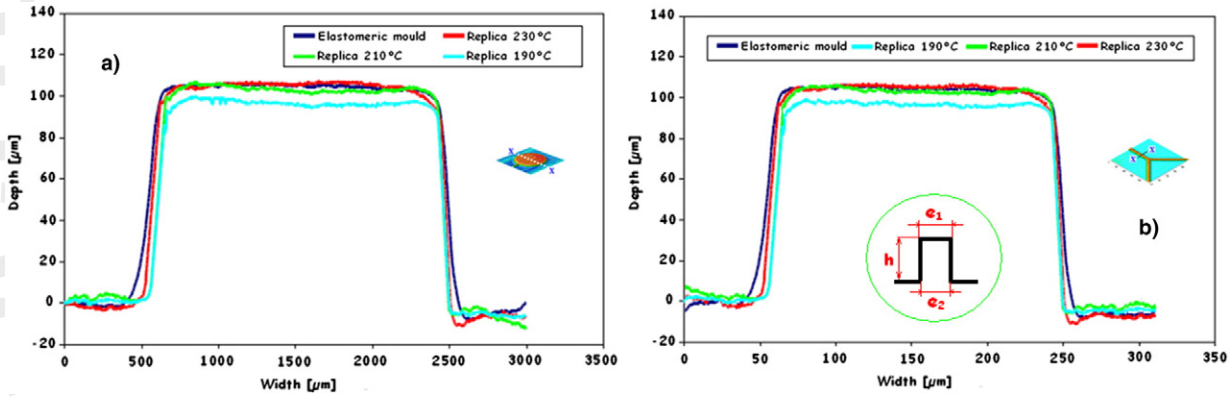

Fig. 15. Comparative 2D profiles of the topography of the nominal profile mould insert (inverted data) and its WC–Co replicas with solid loading of 40%, obtained at various temperatures, corresponding to channel widths of 200 μm (a) and a reservoir diameter of 2000 μm (b) recorded in the X–X direction.

3.2. Preparation and characterisation of the feedstock

The mixing torques were measured and plotted versus time for different cobalt tungsten carbide feedstocks, as shown in Fig. 12. The observed torque peaks are due to the introduction of small amounts of feedstock into the mixture. The mixture with a solid loading of 40% had the lowest torque homogenisation, reaching a value of approximately 0.85 N·m. Therefore, the optimal load of cobalt tungsten carbide powder was identified to be 42%. Beyond 42%, the feedstock did not demonstrate mixability. Instead, the feedstock reached the threshold of mixability, which leads to the formation of inhomogeneous mixtures.

3.3. Hot embossing tests

3.3.1. Effect of the embossing load

Fig. 13 relates typical results concerning the first experimental tests. The feedstocks gradually fill the elastomeric mould cavities as the forming load increases at constant temperature and even during cooling of the cavities. Thus, for a properly defined forming temperature, by increasing the forming load of the feedstock substrate, one can improve and facilitate filling and can improve the surface roughness of the metallic replicas. Hence, the surfaces of the replicated parts were observed to be smooth with $R_a < 1$ μm. This result can be partially related to the forming load increase, which is favourable for decreasing the surface roughness.

3.3.2. Effect of the hot embossing temperature

In Fig. 14, each view corresponds to different filling stages in the development of the cavities and micro channels. At 170 °C, close to the PP melting temperature, the surfaces of the embossed patterns were extremely rough due to the partial melting of the binder system. However, it was observed that the filling ratio increased with increasing forming temperature, yielding an accurate replica of the original imprint.

After several tests, the temperature was observed to have a strong effect on the resulting filling rate and the final surface roughness of the cavities. This trend regarding the related effects can be directly observed in Fig. 8a and d. These experimental results are consistent with the results obtained from other positions of the same sample. This finding could be due to the binder fluidity during hot embossing, which can affect the flow of the feedstock into the detailed parts of the die mould.

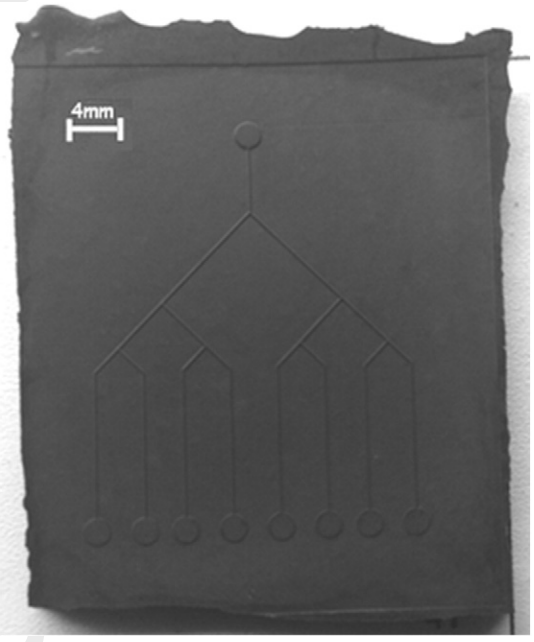

Fig. 16. Photographs of the micro-fluidic samples after the embossing step using two different feedstocks for Co–WC with a solid loading of 38 vol.%.

Table 4
Average depth and widths (h, e_1 and e_2 defined, respectively, as indicated in the scheme) of the channels located at the middle and extremity of the channel length on the WC–Co replicas compared with the dimensions of the corresponding ridges on the elastomeric mould insert.

Channel	Elastomeric mould insert		WC–Co replicas	
	Middle	Extremity	Middle	Extremity
h [μm]	100 ± 1	100 ± 1	98 ± 2	98 ± 3
e_1 [μm]	200 ± 1	200 ± 2	197 ± 3	196 ± 3
e_2 [μm]	200 ± 1	200 ± 1	199 ± 2	198 ± 3

Table 5
Dimensions of the elastomeric mould and micro-sized structures of the micro-fluidic samples (WC–Co sintered at 1000 °C).

Micro-sized structure	Solid loading content		
Dimensions [mm]	40%	42%	44%
	Shrinkage [%]		
Ø = 2	24	23	21
a = 6	24	21	19
b = 14	23	22	20
c = 14	24	20	20
d = 4	24	21	18
e = 14	25	22	20
f = 64	24	23	21
g = 58	24	22	21

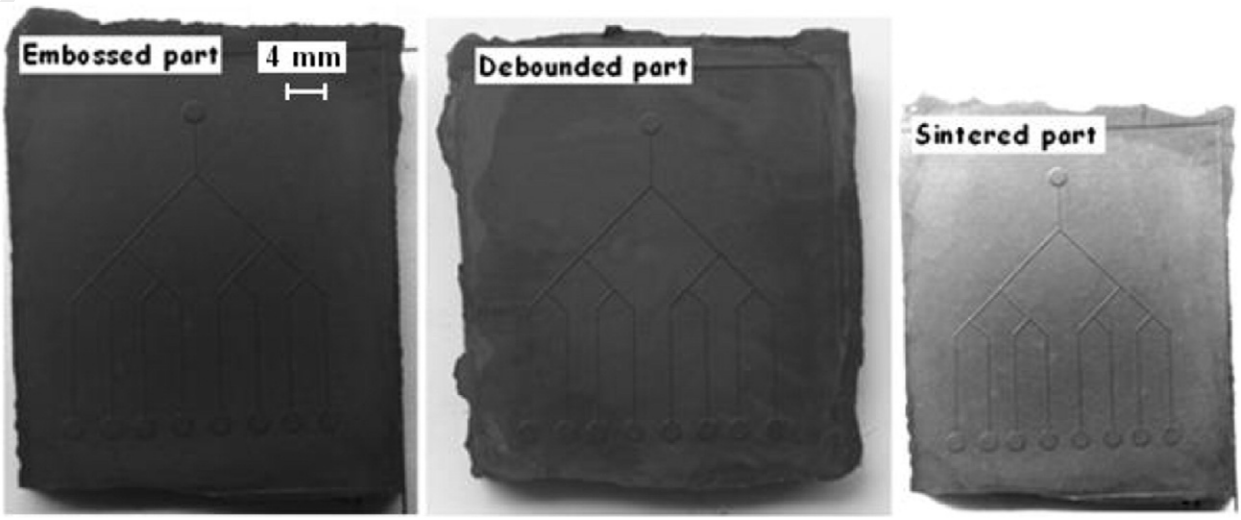

Fig. 17. Photographs of the WC–Co microfluidic replicas with the solid loading of 42 vol.% after different processing steps: (a) embossed to 170 °C, (b) debinded up to 350 °C and (c) sintered up to 1000 °C.

Therefore, at 230 °C, the feedstocks may be pushed by the binders towards the mould details, leaving fewer defects in the final shape. The average surface roughness, Ra, measured at the base of the reservoirs decreased sharply at the melting temperature; then, the R_a values levelled off at higher temperatures (beyond 190 °C), as observed in Fig. 14d.

Metallic replicas of 4 mm thickness were produced using an elastomeric mould insert with a pattern of 100 µm thickness (see Fig. 16). To assess the filling of the elastomeric mould insert and the dimensional and geometrical quality of the replication, 2D profile measurements were performed on the metallic replicas using scanning mechanical microscopy (SMM). The apparatus used was a tactile profilometer with a conical probe in diamond with a tip radius of 2 µm and a cone angle of 45° [8].

The evolutions of the channel profiles of the embossed WC–Co replicas were recorded along the X–X direction. The profiles of the WC–Co replica were quasi-equivalent to the recessed profile and inverted of the studied insert for channel widths and reservoir diameter equal to 200 µm and 2000 µm, respectively. Fig. 15 presents some graphs produced with lines with different widths. Although a constant load was maintained until separation, and no apparent irregularity was observed during the experiment, the SMM profiles indicate the presence

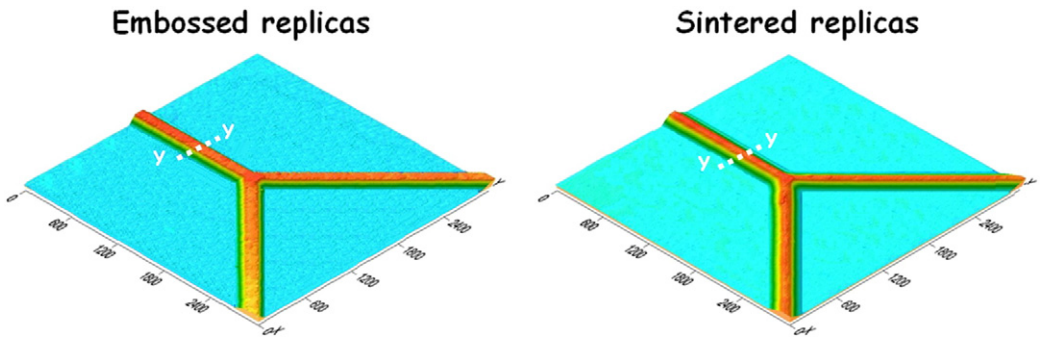

Fig. 18. 3D topographic imprints of WC–Co replicas with a solid content equal to 40 vol.% obtained at various steps (units: µm).

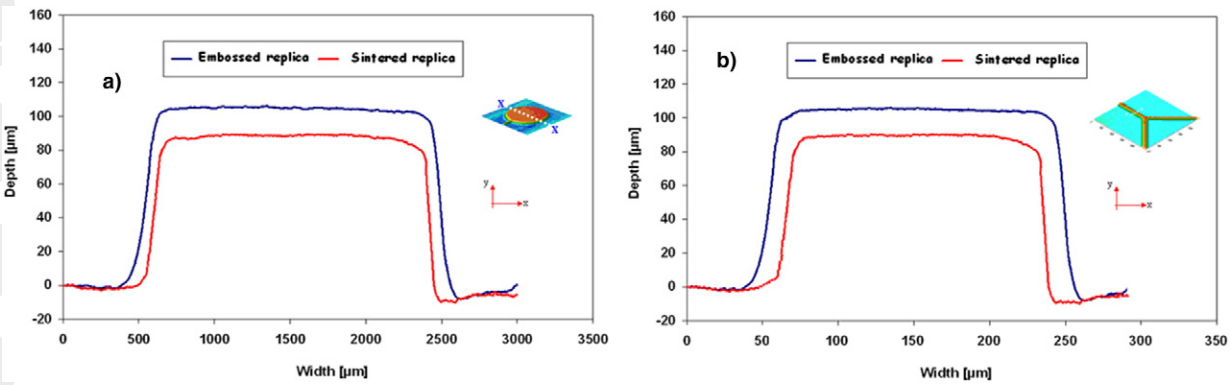

Fig. 19. A comparison of variations in the 2D topographical profiles of the embossed replicas and sintered replicas using WC–Co feedstock (42 vol.%), sampled along the X–X direction (zone 1): (a) reservoir and (b) micro-canal.

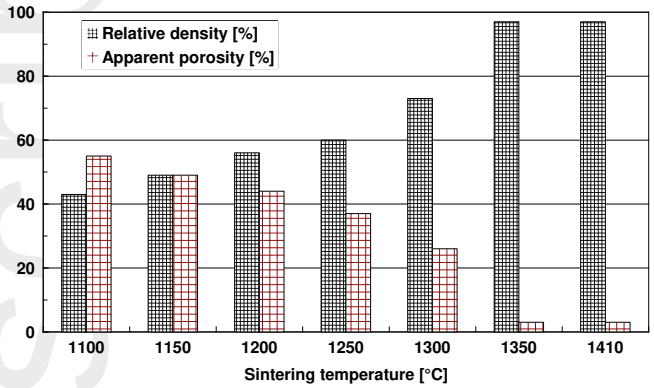

Fig. 20. Variation of the properties of WC–Co hard metal alloys after various sintering temperature treatments: (a) relative density and (b) apparent porosity.

of a distinct trace of the samples after embossing. One must note that the sloped shapes of the cavity sidewalls observed in Fig. 15 are due to the conical shape of the tactile probe (i.e., the probe convolution effect). In reality, these wall profiles are almost vertical. One can conclude that the forming load and temperature values determine the replication accuracy in terms of the width and shape and have a significant effect on the accu racy of the final replication.

Fig. 16 presents a photograph of the micro fluidic samples following the embossed processing step using the different sample types. The samples were obtained under the same conditions. Good shape reten tion without warpage or cracking was achieved following de moulding.

The dimensions (width and depth) of the channels of the replicas produced in the WC Co feedstocks were measured for a batch of ten replicas at two different locations, in the middle of the channel length and at one extremity of the channel length (just before the reservoir). The depth value was measured with SMM, whereas the top and bottom widths were measured optically at the focal plane of the microscope. The results of the average size of the channels on the ten replicated pieces are presented in Table 4.

3.4. Physical properties of the resulting microfluidic replicas

3.4.1. Shrinkage of the resulting micro fluidic specimens

The sizes and dimensions of the final components were measured and compared with the initial geometry of the embossed die mould to qualify the shrinkage with the respective sintering stage (see Fig. 5b). The analyses of the dimensions were performed on the sintered speci mens embossed with the WC Co feedstocks loaded at 40 46% WC Co. The mean shrinkages are listed in Table 4.

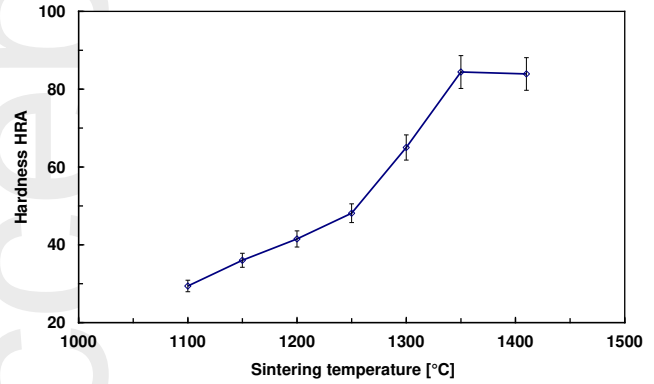

Fig. 21. Variation of the hardness of the WC–Co hard metal alloys after various sintering temperature treatments.

The dimensions of the micro fluidic samples for the three different powder solid loadings are given in Table 5. Compared with the silicon mould insert, the dimensional changes after the sintering stage are clearly evident. The dimensional changes in the length and width of the microstructures indicate similar trends. As an example for the WC Co samples, the shrinkage values were approximately 21% and 24%. However, the width and height of the embossed microstructures decreased gradually as the sintering temperature was increased, regard less of the powders used.

The main parameters affecting the final sample size have been studied already, including the metal powder morphology, binder system ingredi ents and proportions, mixing conditions, mould design, embossing pa rameters, rheological behaviour of the embossing materials, debinding and sintering stages, equipment and even environmental conditions. Among these often integrally related factors, the most sensitive are the solid loading and the mould design [55].

Fig. 17 presents a photograph of the microfluidic components after undergoing different processing steps. On the one hand, analysis of the different microfluidic embossed samples indicates that the use of a higher solid loading of feedstock improves the embossed sample rigid ity with lower thermal stress after demoulding, which results in proper global flatness after demoulding. On the other hand, micro embossing at the lowest temperature with acceptable fidelity can improve the global flatness after demoulding. Comparing the sintered microstruc tures and embossed microstructures, it can be observed that the shape retention of the sintered microstructures has been properly realised. One cannot observe visual defects on the sintered component. Com pared with the embossed component, the dimensional changes after debinding are not noticeable, although the dimensional changes after sintering may be clearly evident.

Fig. 18 shows the surface topography of the metallic replicas, after being embossed then sintered, respectively, while Table 5 provides the corresponding surface micro topography data. The improvement in the surface micro topography by selecting a suitable solid loading, proper embossed temperature and the kinetic control of the densifica tion and atmosphere is further illustrated in Fig. 18.

As demonstrated in Fig. 19, the sintered replicas were approximately 20 μm shallower than the embossed replicas, which is likely due to shrinkage after the sintering step. In this stage, the component un dergoes a low dimensional anisotropic shrinkage in the range of 10 to 12%, according to the thickness and in the range of 19 to 24%, in other directions. This variation is depending on the powder characteristics, solid loading, etc.

3.4.2. Densities and Vickers hardness of the resulting micro fluidic specimens

The densities of the sintered micro fluidic devices were measured using the water displacement method (the Archimedes method) for each of the three feedstocks. Our previous study indicated that when the sintering temperature increased, the relative density rapidly in creased, and the apparent porosity clearly decreased [54,56]. Fig. 20 shows the relative density and apparent porosity of WC Co hard metal alloys after various sintering temperature treatments. The lowest relative density (43.1%) appeared for the 1100 °C sintered WC Co spec imens, as observed in Fig. 20. The relative density was slowly increased to 73.0% as the sintered temperature was increased to 1300 °C. However, when the temperature reached 1350 °C, the relative den sity was rapidly increased to 97.76%. Consequently, the relative den sity of the sintered WC Co alloys can be significantly increased as the sintering temperature is increased. This result also agrees with our previous findings.

The hardness of the specimens was measured using a Rockwell indenter (HRA, Indentec 8150LK) with a loading of 60 kg, which com plied with the CNS 2114 Z8003 standard methods. The hardness mea surements were conducted on the polished sections of the different sintered components. Each area was polished using diamond pastes

with 3 μm and 0.1 μm particle diameters at a rotation speed equal to 150 rpm. Finally, the samples were polished again using a diamond paste of 0.1 μm for approximately 20 s and were then examined with an optical microscope. Fig. 21 shows the mechanical properties test for WC Co hard metal alloys after various sintering temperature treat ments. Fig. 21 illustrates that the hardness of the sintered WC Co alloys rapidly increased as the sintering temperature increased. This finding can be ascribed to the decreased porosities, which result in the increas ing densification and strengthening mechanism. Due to the large num ber of internal pores existing in the 1250 °C sintered WC Co specimens, the hardness is only approximately HRA 48.3 ± 0.6. In addition, the greatest hardness of the WC Co specimens reached HRA 84.2 ± 0.4, which appeared for the 1350 °C sintering for 1 h. The hardness trend is consistent with the porosity. It is reasonable to suggest that the poros ity of the sintered specimens plays an important role in affecting the hardness.

3.4.3. Roughness variation of the micro specimens

Ten measurements at each position were performed, and the average values from these ten measurements were used for analysis and correlation. Fig. 22 shows the variation of surface roughness of the WC Co micro fluidic die moulds during different processing steps. The results indicate that the highest surface roughness ratio (see Table 4) appeared in the 1100 °C sintered WC Co specimens. It is reasonable to suggest that the WC Co alloys sintered at 1100 °C did not achieve full sintering. Therefore, the 1410 °C sintered WC Co alloys represent the smallest surface roughness ratio. When the temperature was increased to 1200 °C and then 1300 °C, the surface roughness ratio of the WC Co alloys was rapidly reduced. The surface roughness ratio appeared in the 1410 °C sintering for 1 h; this result indicated that the sintering temperature was close to the liquid phase sintering temperature [56]. Thus, the sintering temperature approached the liquid phase sintering temperature for tungsten carbides, which would enhance the volume shrinkage ratio and lead to good sintering materials.

Table 6 summarises the roughness coefficients of these measured surfaces, the arithmetical average height, the root mean square height, and the total height (R_a, R_z and R_t, respectively) on the elastomeric mould insert and metallic replicas. The roughness factors ($R_{replica}/R_{mould}$), as determined from measurements in areas (a) and (b), respec tively, are also listed in Table 6, see Fig. 23. Ideally, if the replication pro cess reproduces perfectly well the roughness of the mould insert, the roughness of the replica should be equal to the roughness of the elasto meric mould insert, and the roughness factor should be equal to 1. In this case, the high value of the roughness ratios indicates that the rep lication process under the selected operative conditions does not repro duce faithfully the elastomeric mould insert roughness, in particular in the areas corresponding to the microstructures of the mould insert. A

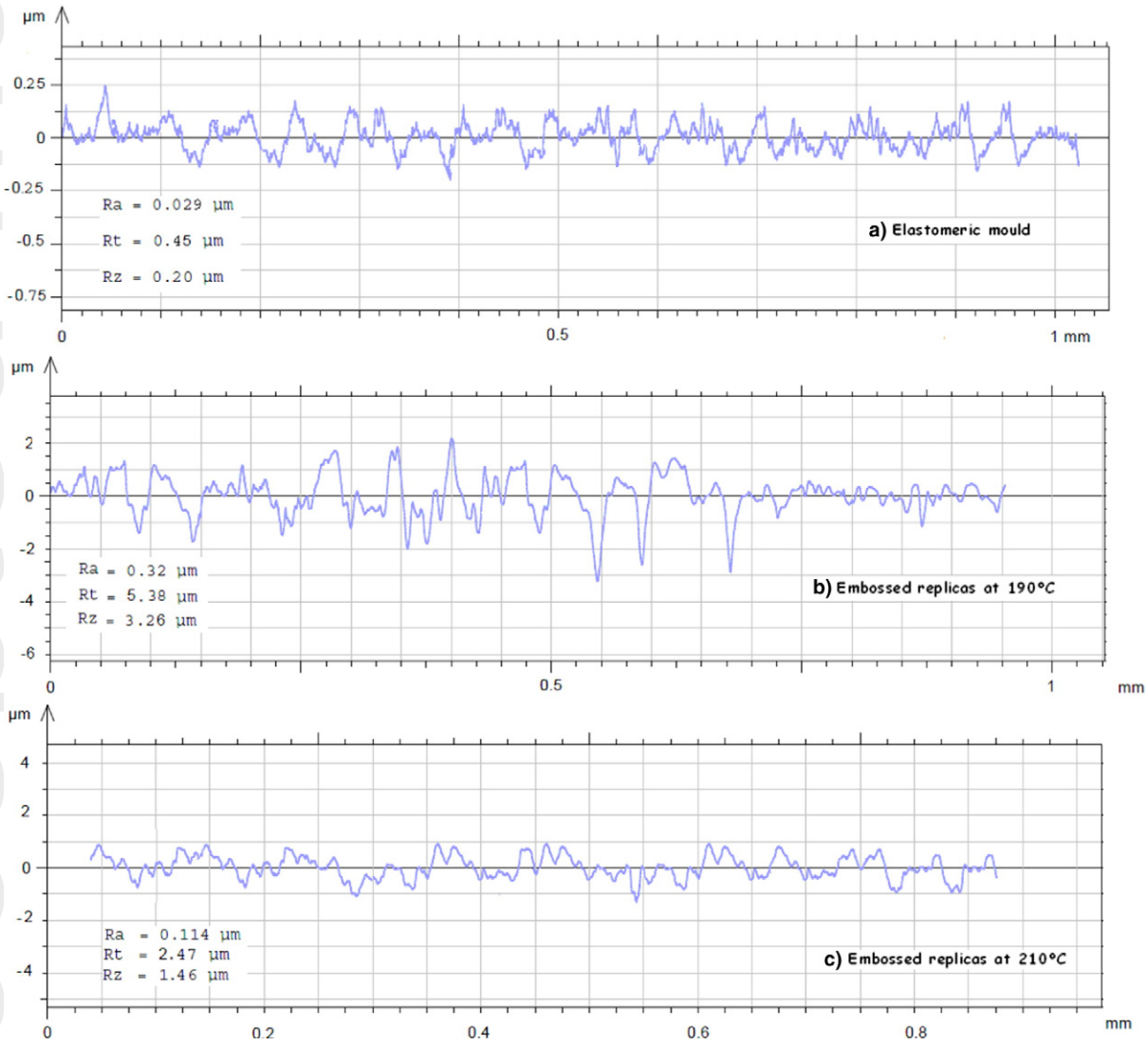

Fig. 22. Variation of surface roughness of the elastomeric mould inserts and the WC–Co micro-fluidic samples at different processing steps (solid loading of 40 vol.%).

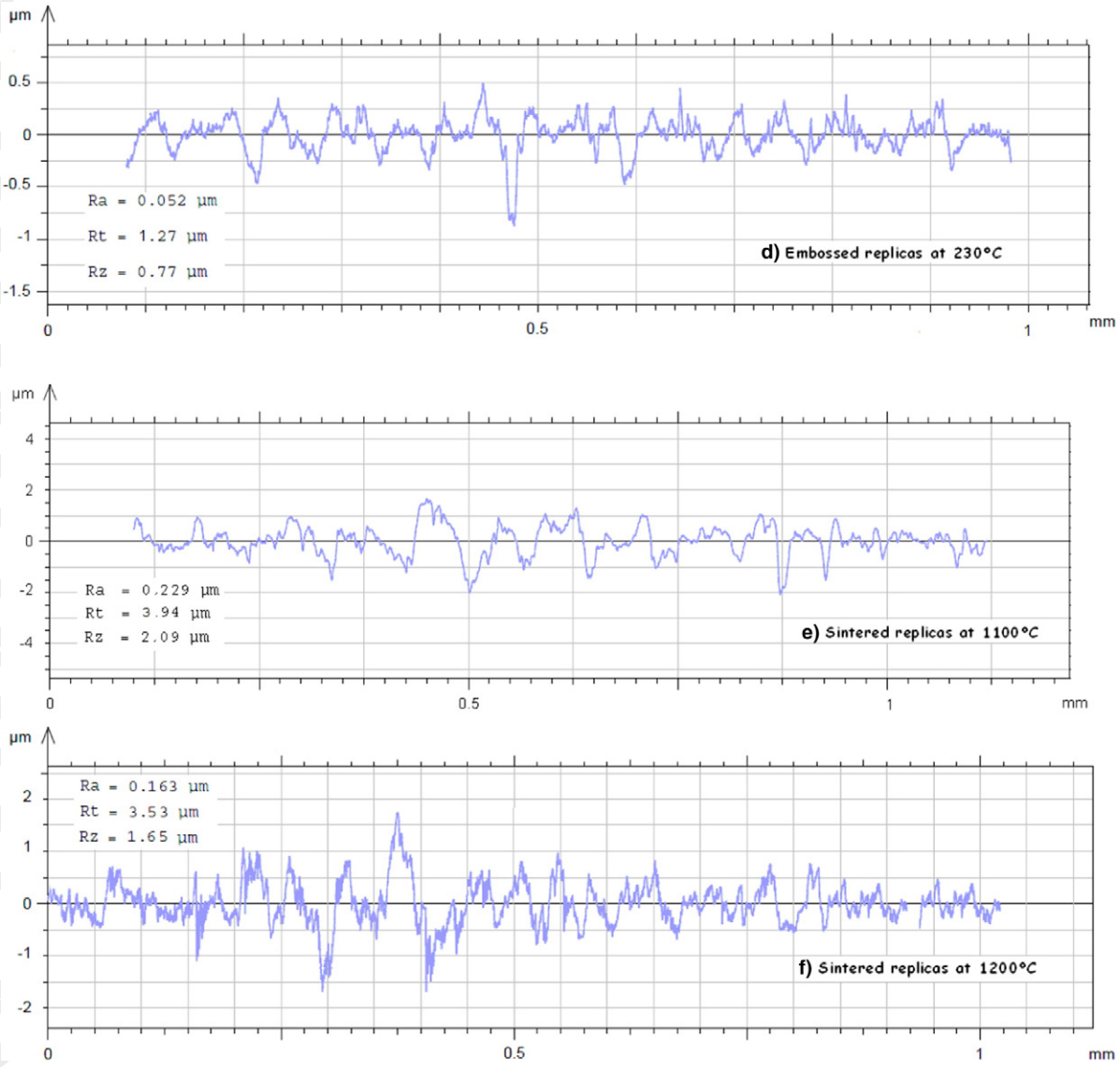

Fig. 22 (*continued*).

decrease of these ratios can be achieved in the hot embossing process using a binder characterised by a very low viscosity compared with that previously used, which would hence fill better the micro cavities of the mould insert. Regarding the sintering process, we can also select the fine powder granulometry (with particle size less than 3.5 µm), leading to perfectly isotropic shrinkage and proper roughness and pos sibly achieve sintering under atmosphere.

4. Conclusions

This paper summarises experimental investigations of the powder hot embossing of micro fluidic die mould cavities based on fine cobalt tungsten carbide powders (D_{50} = 5.7 µm). One binder system used consisted of paraffin wax, polypropylene and stearic acid with relative fractions of 40:55:5. The binder was retained through measurements of thermogravimetric analyses and mixing torques for different sets of material and processing parameters. Currently, the following conclu sions can be drawn:

1) The results from this work clearly indicate that under different mixing conditions and powder loadings, the feedstocks possess different rheological characteristics. The optimum solid loading resulting from the analysis is approximately 40 vol.%, which presents the proper flow conditions suitable for hot embossing and an ab sence of agglomerates due to effective mixing.
2) A complete powder hot embossing process was successfully per formed for the optimum solid loading feedstock. The pressure and forming temperature results for hot embossing indicated that tung sten carbide feedstocks with lower solid powder loadings of 42% ex hibit higher flow stability.
3) The debinding conditions were determined by thermal analysis. Such information can be used to predict both the hot embossing and thermal debinding of the feedstocks. These data demonstrate that hot embossing of the cobalt tungsten carbide feedstock should be performed above 160 °C (i.e., the upper melting temperature) but below 250 °C, beyond which the binder components paraffin wax and stearic acid start degrading.
4) Based on the thermal characterisations of the feedstock, on one hand, a complete powder hot embossing process was successfully per formed for an optimum solid loading feedstock that exhibits lower vis cosity. On the other hand, no distortion occurred in the debounded specimens, and complex components could be manufactured out of

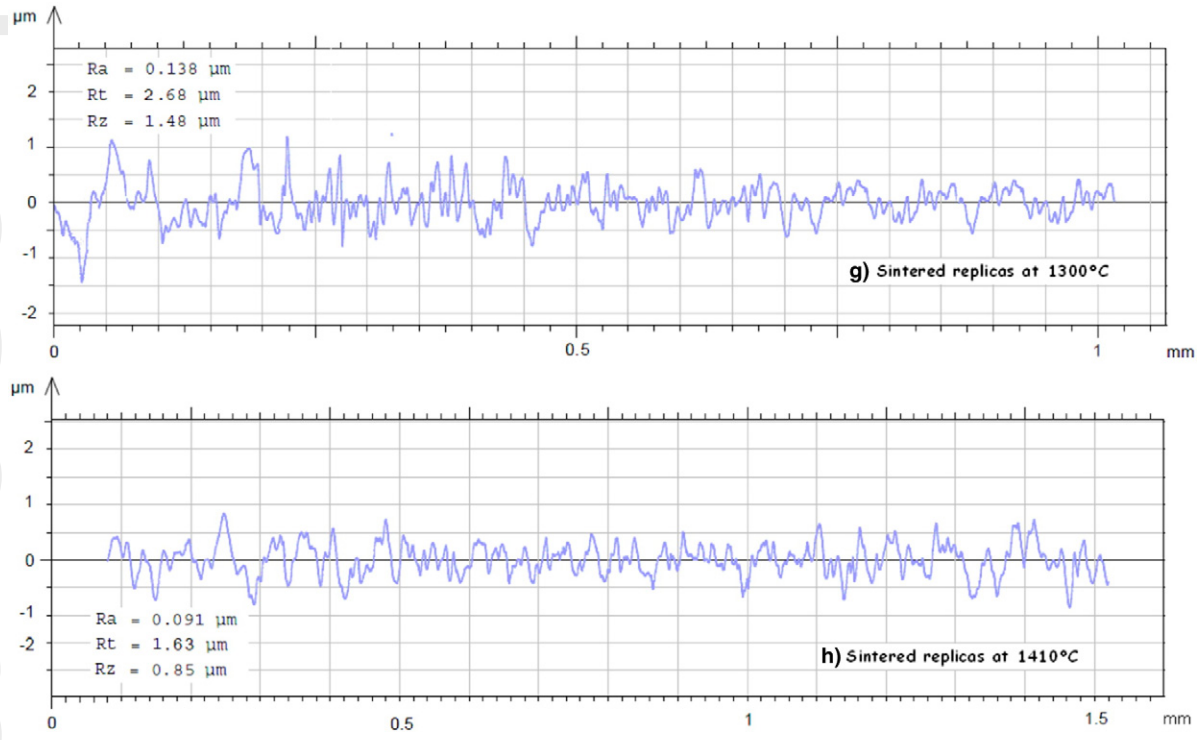

Fig. 22 (*continued*).

the feedstock. The metallic replicas were sintered at temperatures, nearly high enough, at which, the metal particle surfaces bound together to result in a final, 96 97% solid density with neither damage nor distortion of the microstructures.

5) The dimensional accuracy of the final die mould cavity was mainly determined by the geometrical dimension accuracy of the embossing stage. Of all the processing parameters, the solid loading, embossing temperature and sintering temperature resulted in the most important effects on the dimensional accuracies and material properties.

Table 6
Roughness coefficients and roughness ratios of the various surfaces measured in the areas indicated in Fig. 23.

		Arithmetical mean roughness R_a (nm)	Maximum peak roughness R_z (µm)	$R_{replica}/R_{insert}$	
				Area a	Area b
Elastomeric die moulds		29 ± 2	0.20 ± 0.05		
Embossed replicas	190 °C	320 ± 16	3.26 ± 0.4	11.8	10.3
	210 °C	114 ± 6	1.46 ± 0.3	4.2	3.6
	230 °C	52 ± 3	0.77 ± 0.1	1.9	1.6
Sintered replicas	1100 °C	229 ± 15	2.09 ± 0.4	8.5	7.4
	1200 °C	163 ± 6	1.65 ± 0.3	6.1	5.2
	1300 °C	138 ± 6	1.48 ± 0.3	5.1	4.4
	1410 °C	91 ± 5	0.85 ± 0.1	3.3	2.9

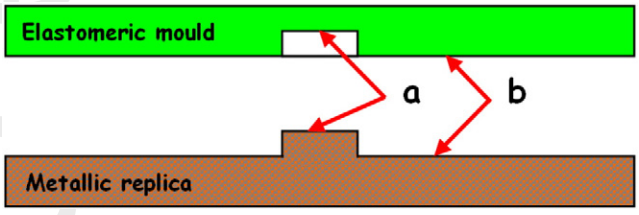

Fig. 23. Schematic representation of the mould insert and replica with the different areas measured (a and b).

In this study, 1350 °C sintered WC Co hard metal alloys were effective in improving the microstructural and mechanical properties after vacuum sintering. The relative density of the WC Co alloys reached 97.76%, and the apparent porosity decreased to 2.21% after 1 h of 1350 °C sintering treatment. In addition, the hardness of the sintered WC Co alloys at 1350 °C was mainly provided by Co (an alloy possessing optimal mechanical properties, including the greatest hardness, HRA 84.2 ± 0.4). This study confirms that the combination of the complementary techniques of UV LIGA processing/casting/hot embossing/powder injection powder provides a low cost and quality microstructured mould tool for plastic microinjection moulding and micro replication by hot embossing.

Further developments and investigations into the powder, feedstock characteristics and sintering process should be performed to obtain high physical and mechanical properties.

References

[1] D. Zhang, B. Su, T.W. Button, Micro-fabrication of three-dimensional, free-standing ceramic MEMS components by soft moulding, Adv. Eng. Mater. 5 (2003) 924–927.
[2] Z. Houming, W. Chengyong, Z. Zhenyu, Dynamic characteristics of conjunction of lengthened shrink-fit holder and cutting tool in high-speed milling, J. Mater. Process. Technol. 207 (2008) 154–162.
[3] U. Şeker, İ. Çiftçi, H. Hasirci, The effect of alloying elements on surface roughness and cutting forces during machining of ductile iron, Mater. Des. 24 (2003) 47–51.
[4] A.K. Ghani, I.A. Choudhury, Husni, Study of tool life, surface roughness and vibration in machining nodular cast iron with ceramic tool, J. Mater. Process. Technol. 127 (1) (2002) 17–22.
[5] J. Steigert, et al., Rapid prototyping of microfluidic chips in COC, J. Micromech. Microeng. 17 (2007) 333–341.
[6] M. Heckele, W.K. Schomburg, Review on micro-molding of thermoplastic polymers, J. Micromech. Microeng. 14 (2009) 1–14.
[7] C.-H. Yang, S.-Y. Yang, A high-brightness light guide plate with high precise double-sided microstructures fabricated using the fixed boundary hot embossing technique, J. Micromech. Microeng. (2013)http://dx.doi.org/10.1088/0960-1317/23/3/035033.
[8] H.N. Hansen, R.J. Hocken, G. Tosello, Replication of micro and nano surface geometries, CIRP Ann. Manuf. Technol. 60 (2011) 695–714.

[9] R.M. McCormick, R.J. Nelson, M.G. Alonso-Amigo, D.J. Benvegnu, H.H. Hooper, Microchannel electrophoretic separations of DNA in injection-molded plastic substrates, Anal. Chem. 69 (1997) 2626–2630.
[10] J.-C. Gelin, T. Barriere, M. Dutilly, Experiments and computational modeling of metal injection molding for forming small parts, CIRP Ann. Manuf. Technol. 48 (1999) 179–182.
[11] G. Lucchetta, M. Fiorotto, P.F. Bariani, Influence of rapid mold temperature variation on surface topography replication and appearance of injection-molded parts, CIRP Ann. Manuf. Technol. 61 (2012) 539–542.
[12] C. Khan Malek, L. Robert, G. Michel, A. Singh, M. Sahli, Manuel B. Gauthier, High resolution thermoplastic rapid manufacturing using injection moulding with SU-8 based silicon tools, CIRP J. Manuf. Sci. Technol. 11 (2011) 382–390.
[13] D.C. Duffy, J.C. McDonald, J.A. Schueller Olivier, G.M. Whitesides, Rapid prototyping of microfluidic systems in polydimethylsiloxane, Anal. Chem. 70 (1998) 4974–4984.
[14] M.T. Gale, Replication techniques for diffractive optical elements, Microelectron. Eng. 34 (1997) 321–339.
[15] M.U. Kopp, H.J. Crabtree, A. Manz, Developments in technology and applications of microsystems, Curr. Opin. Chem. Biol. 1 (1997) 410–419.
[16] H. Becker, W. Dietz, Microfluidic devices for μ-TAS applications fabricated by polymer hot embossing, Proc. SPIE Microfluid. Devices Syst. 35 (1998) 177–182.
[17] M. Worgull, Hot Embossing, Theory and Technology of Microreplication (Micro and Nano Technologies), William Andrew, Burlington, 2009.
[18] H. Becker, U. Heim, Hot embossing as a method for the fabrication of polymer high aspect ratio structures, Sensors Actuators 83 (2000) 130–135.
[19] M. Sahli, C. Millot, C. Roques-Carmes, C. Khan Malek, J.-C. Gelin, T. Barrière, Quality assessment of polymer replication by hot embossing and micro-injection moulding processes using scanning mechanical microscopy, J. Mater. Process. Technol. 209 (2009) 5851–5861.
[20] F. Klocke, H. Kratz, Advanced tool edge geometry for high precision hard turning, Ann. CIRP 48 (2005) 59–62.
[21] Y.K. Chou, H. Song, Tool nose radius effects on finish hard turning, J. Mater. Process. Technol. 148 (2004) 259–268.
[22] G.V. Kaigala, S. Ho, R. Penterman, C.J. Backhouse, Rapid prototyping of microfluidic devices with a wax printer, Lab Chip 7 (2007) 384–387.
[23] A.W. Martinez, S.T. Phillips, G.M. Whitesides, Diagnostics for the developing world: microfluidic paper-based analytical devices, Anal. Chem. 82 (2010) 3–10.
[24] W.K.T. Coltro, D.P. de Jesus, J.A.F. da Silva, C.L. do Lago, E. Carrilho, Toner and paper-based fabrication techniques for microfluidic applications, Electrophoresis 31 (2010) 2487–2498.
[25] P.I. Okagbare, J.M. Emory, P. Datta, J. Goettert, S.A. Soper, Fabrication of a cyclic olefin copolymer planar waveguide embedded in a multi-channel poly(methyl methacrylate) fluidic chip for evanescence excitation, Lab Chip 10 (2010) 66–73.
[26] I.R.G. Ogilvie, V.J. Sieben, C.F.A. Floquet, R. Zmijan, M.C. Mowlem, H. Morgan, Reduction of surface roughness for optical quality microfluidic devices in PMMA and COC, J. Micromech. Microeng. 20 (2010) 065016 (8 pp.).
[27] M. Sahli, C. Millot, J.-C. Gelin, T. Barrière, The manufacturing and replication of microfluidic mould inserts by the hot embossing process, J. Mater. Process. Technol. 213 (2013) 913–925.
[28] Q. Wang, H.Q. Yin, X.H. Qu, J.L. Johnson, Effects of mold dimensions on rheological of feedstock in micro powder injection moulding, Powder Technol. 193 (2009) 15–19.
[29] M. Youseffi, I.A. Menzies, Injection molding of WC–6Co powder using two new binder systems based on montanester waxes and water soluble gelling polymers, Powder Metall. 40 (1997) 62–65.
[30] C. Kung, T.T. Liao, K.H. Tseng, K.Y. Chen, M.S. Chuang, The Influences of powder mixing process on the quality of W–Cu composites, Trans. Can. Soc. Mech. Eng. 33 (2009) 361–375.
[31] J.J. Dumond, H.Y. Low, Recent developments and design challenges in continuous roller micro- and nanoimprinting, J. Vac. Sci. Technol. B 30 (2012) 010801–010828.
[32] J. Meng, N.H. Loh, G. Fu, B.Y. Tay, S.B. Tor, Micro powder injection moulding of alumina micro-channel part, J. Eur. Ceram. Soc. 31 (2011) 1049–1056.
[33] M. Rafi Raza, Faiz Ahmad, M.A. Omar, R.M. German, Effects of cooling rate on mechanical properties and corrosion resistance of vacuum sintered powder injection molded 316L stainless steel, J. of Mater. Process. Technol. 212 (2012) 164–170.
[34] G. Upadhyaya, Materials science of cemented carbides—an overview, Mater. Des. 22 (2001) 483–489.
[35] F. Abdolali, M. Norhamidi, A. Bakar Sulong, R. Javad, Y.N. Wong, Fabrication of cemented tungsten carbide components by micro-powder injection moulding, J. Mater. Process. Technol. 214 (2014) 1436–1444.
[36] M. Yang, R.M. German, Nanophase and superfine cemented carbides processed by powder injection moulding, Int. J. Refract. Met. Hard Mater. 16 (1998) 107–117.
[37] A. Rota, T.V. Duong, T. Hartwig, Wear resistant tools for reproduction technologies produced by micro powder metallurgy, Microsyst. Technol. 7 (2002) 225–228.
[38] C.R. Lin, R.H. Chen, C. Hung, Preventing non-uniform shrinkage in open die hot embossing of PMMA micro-structures, J. Mater. Process. Technol. 140 (2003) 173–178.
[39] Biswajit Saha, Sh.u.B. Tor, Erjia Liu, David E. Hardt, Jung H. Chun, Ti-Al-PTFE coated stainless steel micro-mold via co-sputtering deposition: replication performance and limitation in hot-embossing, Sensors Actuators B Chem. 163 (2012) 290–298.
[40] Shuhuai Lan, Hye-Jin Lee, EunHee Kim, Jun Ni, Soo-Hun Lee, Xinmin Lai, Jung-Han Song, Nak Kye Lee, Moon G. Lee, A parameter study on the micro hot-embossing process of glassy polymer for pattern replication, Microelectron. Eng. 86 (2009) 2369–2374.
[41] J.M. Li, C. Liu, J. Peng, Effect of hot embossing process parameters on polymer flow and microchannel accuracy produced without vacuum, J. Mater. Process. Technol. 207 (2008) 163–171.
[42] Rajeeb K. Jena, C.Y. Yue, Y.C. Lam, Z.Y. Wang, High fidelity hot-embossing of COC microdevices using a one-step process without pre-annealing of polymer substrate, Sensors Actuators B Chem. 150 (2010) 692–699.
[43] M. Sahli, C. Millot, C. Roques-Carmes, C. Khan Malek, J.C. Gelin, T. Barrière, Quality assessment of polymer replication by hot embossing and micro-injection moulding processes using scanning mechanical microscopy, J. Mater. Process. Technol. (2009) 5851–5861.
[44] G. Cheng, M. Sahli, J.-C. Gelin, T. Barrière, Process parameter effects on dimensional accuracy of a hot embossing process for polymer-based micro-fluidic device manufacturing, Inter. J. of Adv. Manuf. Technol. 75 (2014) 225–235.
[45] J. Giboz, T. Copponex, P. Mélé, Microinjection moulding of thermoplastic polymers: a review, J. Micromech. Microeng. 17 (2007) 96–109.
[46] M. Heckele, W.K. Schomburg, Review on micro-moulding of thermoplastic polymers, J. Micromech. Microeng. 14 (2004) 1–14.
[47] G. Fu, S.B. Tor, N.H. Loh, D.E. Hardt, Micro-hot-embossing of 316L stainless steel microstructures, Appl. Phys. 97 (2009) 925–931.
[48] T.S. Srivatsan, R. Woods, M. Petraroli, T.S. Sudarshan, An investigation of the influence of powder particle size on microstructure and hardness of bulk samples of tungsten carbide, Powder Technol. 122 (2002) 54–60.
[49] Y. Xia, et al., Replica moulding using polymeric materials: a practical step toward nanomanufacturing, Adv. Mater. 9 (1997) 147–149.
[50] J.S. Kim, K. Jiang, I. Chang, Pressure free fabrication of 3D micro-components using Al powder, Adv. Eng. Mater. 8 (2006) 38–41.
[51] M. Imbaby, K. Jiang, I. Chang, Fabrication of 316-L stainless steel micro parts by soft lithography and powder metallurgy, Mater. Lett. 62 (2008) 4213–4216.
[52] Z. Zhu, X. Wei, K. Jiang, A net-shape fabrication process of alumina micro-components using a soft lithography technique, J. Micromech. Microeng. 17 (2007) 193–198.
[53] S.H. Chang, T.P. Tang, K.T. Huang, F.C. Tai, Powder Metall. 54 (2011) 507–512.
[54] S.H. Chang, S.C. Lee, C.H. Tam, K.T. Huang, C. Liang, F.C. Tai, Powder Metall. 54 (2011) 325–330.
[55] N.H. Lohand, R.M. German, Statistical analysis of shrinkage variation for powder injection moulding, J. Mater. Process. Technol. 59 (1996) 278–284.
[56] S.H. Chang, S.H. Chen, K.T. Huang, Mater. Trans. 53 (2012) 1689–1694.